

Alzheimer's genetic risk factor *FERMT2* (Kindlin-2) is regulated by risk allele-binding of miR-4504 and leads to synaptic dysfunction in an APP-dependent manner

Fanny Eysert¹, Audrey Coulon¹, Emmanuelle Boscher^{2,3}, Anaïs-Camille Vreulx¹, Amandine Flaig¹, Tiago Mendes¹, Sandrine Hughes⁴, Benjamin Grenier-Boley¹, Xavier Hanouille⁵, Florie Demiautte¹, Charlotte Bauer⁶, Mikael Marttinen⁷, Mari Takalo⁷, Philippe Amouyel¹, Shruti Desai¹, Ian Pike⁸, Mikko Hiltunen⁷, Frédéric Chécler⁶, Melissa Farinelli⁴, Charlotte Delay¹, Nicolas Malmanche¹, Sébastien Hébert^{2,3}, Julie Dumont¹, Devrim Kilinc¹, Jean-Charles Lambert^{1,#} and Julien Chapuis^{1,#}

These authors share the last authorship

1. Univ. Lille, Inserm, CHU Lille, Institut Pasteur de Lille, U1167 - RID-AGE - Facteurs de risque et déterminants moléculaires des maladies liées au vieillissement, Lille 59019 France
2. Centre de recherche du CHU de Québec-Université Laval, CHUL, Axe Neurosciences, Québec, Canada
3. Faculté de médecine, Département de psychiatrie et de neurosciences, Université Laval, Québec, Canada
4. E-PHY-SCIENCE, Bioparc de Sophia Antipolis, 2400 route des Colles, Biot 06410 France
5. Univ. Lille, CNRS, UMR8576 - Labex DISTALZ, Villeneuve d'Ascq 59655 France
6. Université Côte d'Azur, Institut National de la Santé et de la Recherche Médicale, Centre National de la Recherche Scientifique, IPMC, Team Labeled "Laboratory of Excellence (LABEX) DistAlz", Valbonne, France
7. Institute of Biomedicine, University of Eastern Finland, Kuopio, Finland
8. Proteome Sciences plc, Hamilton House, London WC1H 9BB, United Kingdom

Corresponding author:

Julien Chapuis, PhD

Inserm UMR1167, Institut Pasteur de Lille, 1 rue du Pr. Calmette, Lille 59019 France

Tel: + 33 3 20 87 78 01

Fax: + 33 3 20 87 78 94

E-mail: julien.chapuis@pasteur-lille.fr

ABSTRACT

We combined genome-wide high-content screenings to identify miRNAs ($n = 2,555$) and target genes ($n = 18,107$) involved in the APP metabolism. This approach highlighted *FERMT2* (or Kindlin-2), a genetic risk factor of Alzheimer's disease (AD). *FERMT2* down-regulation by multiple miRNAs modulated APP metabolism and increased A β secretion. Among these, miR-4504, which is over-expressed in AD brains, decreased *FERMT2* expression depending on the presence of the deleterious rs7143400 variant. Decreased *FERMT2* expression altered both axonal growth and long-term potentiation in an APP-dependent manner. Overall, this work provides important mechanistic insight on the roles of *FERMT2* and miRNAs in APP biology.

INTRODUCTION

AD is a neurodegenerative disease characterized by two main pathological hallmarks: (i) intracellular neurofibrillary tangles consisting of hyper-phosphorylated Tau proteins and (ii) extracellular amyloid plaques consisting of aggregates of β -amyloid (A β) peptides resulting from the processing of amyloid precursor protein (APP). Three main proteases (α -, β - and γ - secretases) are involved in APP processing through (i) the amyloidogenic pathway (β - and γ -secretases), leading to A β production, and (ii) the non-amyloidogenic pathway (α - and γ -secretase), which prevents A β generation by cleaving APP within the A β sequence (Checler 1995).

The identification of early-onset autosomal dominant AD-linked mutations in the genes for *APP* and presenilin (*PS1* and *PS2*, part of the γ -secretase), but also late-onset sporadic AD-linked mutations in *ADAM10* (carrying part of the α -secretase activity in the brain) (Kim et al. 2009), have placed abnormal APP metabolism at the center of the disease, further supporting the amyloid cascade hypothesis (Hardy 1997; Hardy & Selkoe 2002): the overproduction of A β peptides –especially the longer forms that are thought to be more neurotoxic– may lead to (or favor) Tau pathology and subsequent neuronal death.

Although the validity of the amyloid cascade hypothesis is strongly debated (Morris et al. 2018), the importance of APP has recently been emphasized by the discovery of a rare *APP* mutation hampering A β production that lowers AD risk (Jonsson et al. 2012). Recent high-throughput genomic approaches have also highlighted APP metabolism in the AD pathophysiological process: the main actors of APP metabolism, e.g., *ADAM10* and *APH1B* (part of the γ -secretase complex), have been characterized as genetic determinants (Jansen et al. 2019; Kunkle et al. 2019), and numerous other genetic determinants have been described as potential modulators of APP metabolism (for a review, see (Dourlen et al. 2019)). Taken together, these genetic data strongly suggest that APP metabolism regulation and consequently APP function still need to be better understood to decipher the AD pathophysiological processes.

Previously, we have used a high content screening (HCS) approach that allowed us to test the impact of 18,107 genes on APP metabolism using short interfering RNA (siRNA) pools (Chapuis et al. 2017). One can argue that endogenous mechanisms regulating the expression of such key players of APP metabolism may be also of importance in the development of the AD processes. Among the different mechanisms involved in gene regulation, microRNAs (miRNAs) appeared of particular interest for several reasons: (i) miRNAs are abundantly expressed in the brain and it is now well established that specific miRNAs expression is altered in AD brain (Hébert et al. 2008; Patrick et al. 2017), (ii) several of these miRNAs have been already implicated in APP metabolism (Delay et al. 2016; Z. Li et al. 2017; Long et al. 2019); (iii) miRNAs have been implicated in various neuronal functions including synaptic plasticity, memory formation and neuron survival which are relevant in the AD context (Schratt 2009; Delay et al. 2012).

With this in mind, we extended our previous HCS approach to identify miRNAs modulating APP metabolism, and by extension key endogenous factors implicated in APP metabolism. This approach led us to characterize 180 genes targeted by 41 miRNAs. Among these genes, we focused on *FERMT2*, a known genetic risk factor of sporadic AD.

METHODS

Cell culture

Human HeLa (RRID:CVCL_0030) and HEK293 (RRID:CVCL_0045) cells were respectively maintained in Eagle's minimal essential medium (American Type Culture Collection, Teddington, UK) and DMEM/Ham's F-12 1:1 medium (Life Technologies, Carlsbad, CA) supplemented with 10% heat-inactivated fetal bovine serum and 2 mM L-glutamine, penicilline (10 UI/mL)/Streptomycine (10 µg/mL).

High-content miRNA screening

The miRNA library (2,555 miRNA mimics, mirVana™ library, Ambion, Austin, TX) was screened in HEK293 cells stably over-expressing mCherry-APP695^{wt}-YFP (**Supplementary Fig. 1**) according to a previous protocol (Chapuis et al. 2017). Briefly, each miRNA (50 nM) was first transferred to 384-well with D-PBS containing 0.1 µl of Lipofectamine RNAiMax (Life Technologies). Then approximately 3,000 HEK293-mCherry-APP695^{wt}-YFP cells were distributed in each well and incubated for 3 d at 37°C. After removal of the cell medium and Hoechst staining, cells were fixed using 10% formalin before image acquisition using an InCell Analyser 6000 (GE Healthcare, Chicago, IL) high-resolution automated confocal microscope.

A customized image analysis software (Columbus 2.7; PerkinElmer, Villebon-sur-Yvette, France) was used for the image analysis and quantification as reported previously (Chapuis et al. 2017). The mean fluorescence intensity of each signal was normalized with the fold change induced by the non-targeting miRNA in the same plate. To evaluate the impact of each miRNA, an average of 1,000 cells were analyzed per run (n = 3). For quality control, we used strictly standardized mean difference with β -score > 3 based on two separate controls (siRNA-APP and miR-NT, **Supplementary Fig. 1**).

In silico prediction of miRNA targets and functions

Seven publicly-available algorithms were used for the prediction of miRNA-targeted genes in the brain: DIANA-microT-CDS (v5.0, r21) (Paraskevopoulou et al. 2013), MiRanda (August 2010 release) (John et al. 2004), mirDB (v5.0) (Wong & Wang 2015), miRTarBase (v6.1) (Hsu et al. 2011), rna22 (v2.0) (Miranda et al. 2006), TargetMiner (May 2012 release) (Bandyopadhyay & Mitra 2009), and TargetScan (v7.1) (Agarwal et al. 2015). In order to minimize false-positive predictions, miRNA-targeted genes were defined as genes predicted by at least 4 out of the 7 algorithms used. To predict the function(s) of miRNAs that target these genes, pathway enrichment analysis was performed using DIANA Tools mirPath (v3.0) (Vlachos et al. 2015).

Luciferase reporter assays

The *FERMT2* 3'-UTR sequence was inserted downstream of the luciferase gene in the psiCHECK2 vector (Promega, Madison, WI, USA), as previously described (Delay et al. 2016). Cells were transfected with a miRNA mimic (Ambion) and psiCHECK2/3'-UTR (Promega, Charbonnières-les-Bains, France). Forty-eight hours after transfection, cells were lysed and luciferase activity was measured using the Dual-Glo® Luciferase Assay System (Promega) and a Wallac 1420 Victor luminometer (PerkinElmer) according to the manufacturer's instructions.

RFLP genotyping

Genomic DNA in the vicinity of the rs7143400 was amplified by PCR using the following primers 5'-GGTTGGGTGTGAATAGGAAT-3' and 5'-TGCATGCCTGATTTATTTGG-3' before digestion with Tsp45I enzyme (Thermo Scientific). Finally, treated PCR products were analyzed in 2% agarose gel to visualize the cleavage bands.

Designing CRISPR/Cas9 and genome editing

gRNA sequences were predicted by Benchling (<http://www.benchling.com>) and cloned into the GeneArt CRISPR OFP Nuclease Vector (ThermoFischer Scientific) allowing Cas9 and gRNA expression. Homology directed repair was induced by co-transfection of 71 pb double-strained DNA oligonucleotide template including rs7143400-T allele in HEK293 cells (**Supplementary Fig. 4**). HEK293 clones were isolated by limiting dilution before RFLP genotyping. Sequence integrity of the *FERMT2* 3'UTR and predicted potential off-target site were validated by Sanger sequencing (**Supplementary Fig. 4**).

Microfluidic chip fabrication

Multicompartment microfluidic devices were used that isolate axons from their cell bodies (Blasiak et al. 2015). PDMS (polydimethylsiloxane) prepolymer was mixed with curing agent (9:1 ratio) according to the manufacturer's recommendations (Sylgard 184 Silicone Elastomer Kit; Dow Corning, Midland, MI) and degassed under vacuum. Then, the PDMS was poured onto a polyester resin replicate (polyglass 26/71, Esprit Composite, Paris, France) and cured 2 h at 70°C. The PDMS pad was detached from the replicate and access wells were punched out using biopsy punches (Harris Uni-Core; Merck, Darmstadt, Germany). Devices were irreversibly bonded to glass coverslips via O₂ plasma (Diener, Ebhausen, Germany). The devices were placed in plastic Petri dishes, UV sterilized for 30 min, and wetted with sterile dH₂O.

Primary neuronal culture and viral transductions

Primary neuronal cultures were obtained from hippocampus or cortices of post-natal (P0) rats as described previously (Kaech & Banker 2006). Briefly, after the dissection of the brains, hippocampi were washed three times in HBSS (HBSS, 1 M HEPES, penicilline/streptomycine, 100 mM sodium

pyruvate; Gibco) and were dissociated via trypsin digestion (2.5%, 37°C; Gibco) for 7 min. Next, hippocampi were incubated with DNase (5 mg/mL; Sigma) for 1 min and washed again in MEM medium supplemented with 10% SVF, 1% Glutamax, 0.8% MEM vitamins, 0.5% penicilline/streptomycine and 0.45% D-glucose (Sigma). With a pipette, hippocampi were mechanically dissociated and resuspended in Neurobasal A medium (Gibco) supplemented with 2% B27 (Gibco) and 0.25% GlutaMax. 200,000 neurons were seeded per well in 24-well plates. 50,000 neurons were seeded in the somatic chamber of microfluidic devices, pre-coated with poly-L-lysine (0.1 mg/mL; Sigma) in borate buffer (0.31% boric acid, 0.475% sodium tetraborate, pH = 8.5). 0.1% EDTA (in H₂O) was added to the Petri dishes containing microfluidic devices to minimize evaporation. The culture medium was refreshed every 3 d. Neurons were maintained at 37°C in a humidified 5% CO₂ incubator.

Lentiviral transductions

Lentiviral transductions were carried out at 1 day in vitro (DIV1) with a multiplicity of infection (MOI) of 10. In the case of co-transduction, MOI of 5 was used for each lentivirus. Briefly, lentiviruses were diluted in culture medium containing 4 µg/mL polybrene (hexadimethrine bromide; Sigma) and were added to the cells. After 6 h of transduction, lentivirus suspension was replaced with fresh medium. The following lentiviruses were used for transduction: Mission shRNA vectors (Sigma) shNT (Non-Mammalian shRNA Control, SHC002), shFERMT2 (TRCN0000191859), shAPP (TRCN0000006707) and pLenti6 empty vectors (Mock) or including human FERMT2^{WT} or FERMT2^{QW} cDNA sequences. LifeAct-Ruby lentivirus (pLenti.PGK.LifeAct-Ruby.W: RRID:Addgene_51009) was a kind gift from Rusty Lansford.

Immunoblotting and A β quantification

Equal amounts (10-25 µg) of cell lysate were collected in RIPA buffer (1 M Tris, 1.5 M NaCl, 0.1% NP-40, 10% SDS, 100 mM sodium orthovanadate, 0.5% sodium deoxycholate, pH = 7.4) containing protease inhibitors (Complete mini; Roche Applied Science, Penzberg, Germany), lithium dodecyl sulfate (LDS), and reducing agent (Invitrogen). Samples were denaturated and analyzed using SDS-PAGE and the following antibodies: human FERMT2 (RRID:AB_10727911), amyloid precursor protein C-terminal domain (RRID:AB_258409), actin (RRID:AB_476692), β -amyloid clone 6E10 (RRID:AB_662798), β -amyloid clone 4G8 (RRID:AB_662812), Synaptophysin I (RRID:AB_887824), PSD95 (RRID:AB_2619800), GAPDH (RRID:AB_10615768). Extracellular culture media were collected in order to dose secreted A β using Alpha-LISA assays (AlphaLISA Amyloid β_{1-x} Kit, AL288C, PerkinElmer) according to the manufacturer's instructions.

Live-cell microscopy for axon elongation and actin dynamics

After DIV5, once the axons reached the axonal chamber of microfluidic devices, the culture medium was replaced with Neurobasal A without phenol red, supplemented with GlutaMax, 2% B₂₇, and 25 mM HEPES. Phase-contrast images of growing axons were acquired every 10 min for 110 min using Zeiss AxioObserver Z1 microscope equipped with a Prime 95B Scientific CMOS (Photometrics, Tucson,AZ) camera and 32× objective. Movies were analyzed using Fiji MTrack J Plugin (Meijering et al. 2012) to determine the axon growth speed.

To visualize filamentous actin (F-actin) dynamics in the growth cones of elongating axons, neurons were co-transduced with LifeAct-Ruby at DIV1. At DIV5, growth cones expressing LifeAct-Ruby were imaged using a Nikon microscope equipped with Yokogawa spinning disk system and a Nikon CFI Apochromat 100× TIRF objective (NA 1.49), in live superresolution mode (66 nm/px). Processed movies were analyzed using Imaris (Bitplane, Zurich, Switzerland) surface tracking tool which reports the speed and direction of F-actin puncta undergoing actin retrograde flow.

Immunofluorescence and PLA

Cells were fixed in 4% paraformaldehyde (PFA) for 15 min, washed 3× with PBS, and permeabilized for 5 min with 0.3% Triton X-100. Cells were incubated with 5% normal donkey serum for 2 h at RT before overnight incubation with the following primary antibodies: human FERMT2 (RRID:AB_10727911), Kindlin2 (RRID:AB_2278298), amyloid precursor protein C-terminal domain (RRID:AB_258409), APP A4 clone 22C11 (RRID:AB_94882), Synaptophysin I (RRID:AB_887824), PSD95 (RRID:AB_2619800), Homer (RRID:AB_2631222), α -Tubulin (RRID:AB_2210391). The cells were then washed 3× with PBS and incubated with the following secondary antibodies raised in donkey (AlexaFluor-conjugated AffiniPure Fragment 405, 488, 594 or 647, Jackson ImmunoResearch), 1:10,000 Hoechst 33342, or 1/40 SiR-Actin probe (SC001, Spirochrome). Alternatively, Kindlin2 (RRID:AB_2278298) and APP A4 22C11 (RRID:AB_94882) antibodies were used for proximity ligation assay (PLA) according to manufacturer's instructions (Duolink®, Olink Bioscience).

Visualisation of miRNA expression at the single-cell level

To visualize RNA molecules by fluorescence at single-cell resolution and quantify gene expression, we used ViewRNA Cell Plus Assay kit (ThermoFischer Scientific) according to the manufacturer's instructions. Briefly, after fixation and permeabilization, cells were washed 3× with PBS containing RNase inhibitor and were incubated with probes directed against specific mRNA or miRNA for 2 h at 40°C. After washes, probes were amplified, first, in a pre-amplifier solution and secondly, in an amplifier solution, both for 1 h at 40°C. Then, cells were incubated with nucleotide probes stained with different fluorophores allowing the detection of mRNA or miRNA puncta. This approach was coupled with immunofluorescence experiments described.

miR quantification in human brain samples

This study was approved by CHU de Québec – Université Laval Research Ethics Committee (#2017-3017). Frozen human brain tissue (0.5–1.2 g per sample) was obtained from the Harvard Brain Tissue Resource Center in Belmont, USA, the Brain Endowment Bank in Florida, USA, and the Human Brain and Spinal Fluid Resource Center in Los Angeles, USA, via NIH Neurobiobank. The cohort of patients included non-dementia controls (N = 30) and AD cases (N = 52), based on neuropathological diagnosis. Upon receipt of the specimens, frozen post-mortem parietal cortex (BA39) was crushed using a biopulverizer prior to RNA extraction and analysis.

Total RNA was extracted from brain tissue (**Supplementary Table 2**) using TRIzol reagent (Ambion, 15596018) according to the manufacturer's instructions. miRNA quantifications were done using the TaqMan miR Reverse Transcription Kit (Applied Biosystem, Burlington, Canada) and TaqMan Universal Master Mix (Applied Biosystem, 4324018) following the manufacturer's instructions. Primers were purchased from ThermoFisher (miR-4504 ID: 464271_mat; RNU48 ID: 001006; miR-222-3p ID: 002276). MiR-4504 and miR-222 levels were normalized to RNU48. The relative amounts of each mature miRNA were calculated using the comparative Ct ($2^{-\Delta\Delta Ct}$) method (Smith et al. 2011).

Cell surface Biotinylation

HEK293-APP^{695WT} cells were transfected with PCDNA4.1, FERMT2^{WT} or FERMT2^{QW} (PCDNA4/HisMax, ThermoScientific V86420) for 48 h. Next, cell surface proteins were biotinylated using sulfo-NHS-SS-biotine (sulfo-succinimidyl-20(biotinamido)ethyl-1,3-dithiopropionate) for 30 min at 4°C according to the manufacturer's instructions (Cell Surface Protein Isolation Kit, Pierce, 89881). Then, cells were lysed and immunoprecipitated with streptavidin beads. Precipitated proteins were eluted from the beads with loading buffer containing 50 mM DTT, heated for 10 min at 95°C and analyzed by WB.

Co-Immunoprecipitation

Equal amounts of protein were collected in co-immunoprecipitation buffer (10 mM HEPES, 140 mM NaCl, 0.5% NP-40, pH = 7.4) containing protease inhibitors (Complete mini, Roche Applied Science) and phosphatase inhibitor (100 mM sodium orthovanadate) and incubated with the primary β -amyloid antibody clone 4G8 (RRID:AB_662812) overnight, with gentle rocking. Production of recombinant C100 fragment was performed as previously described (Sevalle et al. 2009). Co-immunoprecipitation was carried out using Pierce Protein A/G magnetic beads kit (Thermo Scientific, 88802) according to the manufacturer's instructions. Samples with proteins and antibody complexes were incubated with 25 μ L (0.25 mg) of A/G magnetic beads previously washed with co-immunoprecipitation buffer. After 1 h of incubation at 4°C, the magnetic beads were washed 3 \times , resuspended with loading buffer (LDS and reducing agent) for 10 min at RT, and analyzed by WB.

Synaptosome extraction

To verify the presence of proteins at the synaptic level we did a subcellular fractionation as previously described (Frandemiche et al. 2014). Briefly, cortical neurons were resuspended in a solution (0.32 M sucrose and 10 mM HEPES, pH = 7.4) and were centrifuged at $1,000\times g$ for 10 min to remove nuclei and debris. The supernatant was centrifuged at $12,000\times g$ for 20 min to remove the cytosolic fraction. The pellet was resuspended in a second solution (4 mM HEPES, 1 mM EDTA, pH = 7.4) and was centrifuged $2\times$ at $12,000\times g$ for 20 min. The new pellet was resuspended in a third solution (20 mM HEPES, 100 mM NaCl, 0.5% Triton X-100, pH = 7.2) for 1 h at 4°C and centrifuged at $12,000\times g$ for 20 min. The supernatant collected corresponds to the non-PSD fraction (Triton-soluble). The remaining pellet was resuspended in a fourth solution (20 mM HEPES, 0.15 mM NaCl, 1% Triton X-100, 1% deoxycholic acid, 1% SDS, pH = 7.5) for 1 h at 4°C and was centrifuged at $10,000\times g$ for 15 min to obtain a supernatant containing the PSD fraction (Triton-insoluble). The different fractions were then analyzed by WB.

Lentivirus injection

For stereotactic injections, C57Bl6/J mice (RRID:IMSR_JAX:000664) were anesthetized with 4% isoflurane (2 L/min) and placed in a stereotaxic frame (68528, RWD Life Science, Shenzhen, China) in which the head of the animal was fixed with a pair of ear bars and a perpendicular tooth bar. During surgical procedures 1.5% isoflurane (2 L/min) was delivered through a facial mask via spontaneous respiration. Their body temperature was maintained between 36.5 and 37.5°C with a homeothermic blanket. Head was shaved and Vetedine was applied. Wounds and pressure points were infiltrated with lidocaine. A skin incision was made along the sagittal midline of the scalp. Craniotomy was made to target our structures of interest. Lentiviruses were injected in right and left hippocampus ($1.5\ \mu\text{L}$ per hemisphere; $0.2\ \mu\text{L}/\text{min}$). After injections, wound clips were used for skin closure. For the sham group, surgical procedures were performed without any injection. During the surgery, the level of anesthesia was regularly verified by testing the nociceptive hind limb withdrawal reflex. Subjects were then allowed to recover in their home cages for at least 7 d before sacrifice for ex-vivo electrophysiological recordings.

Hippocampal acute slices preparation

One week after the surgery, sagittal hippocampal brain slices were obtained using standard brain slicing methods. Mice were deeply anesthetized with isoflurane and decapitated. The brain was quickly removed and immersed in ice-cold pre-oxygenated artificial cerebrospinal fluid (aCSF) containing: 124 mM NaCl, 3.75 mM KCl, 2 mM MgSO_4 , 2 mM CaCl_2 , 26.5 mM NaHCO_3 , 1.25 mM NaH_2PO_4 , 10 mM Glucose, continuously oxygenated (pH = 7.4; 27°C). $350\ \mu\text{m}$ -thick slices were prepared using a Vibratome (VT 1000S; Leica Microsystems, Bannockburn, IL), and placed in a

holding chamber filled with aCSF. Slices were allowed to recover in these conditions at least 1 h before recording.

Electrophysiological recordings

For electrophysiological recordings, a single slice was placed in the recording chamber, submerged and continuously superfused with gassed (95% O₂, 5% CO₂) aCSF at a constant rate (2 mL/min). Extracellular fEPSPs were recorded in the CA1 stratum radiatum using a glass micropipette filled with aCSF. fEPSPs were evoked by the electrical stimulation of Schaffer collaterals/commissural pathway at 0.1 Hz with a glass stimulating electrode placed in the stratum radiatum (100 μ sec duration).

To test the effect of miRNA-expressing lentiviruses on basal synaptic transmission, Input/Output (I/V) curves were constructed at the beginning of the experiment. The slope of fEPSPs was measured and plotted against different intensities of stimulation (from 0 to 100 μ A).

Stable baseline fEPSPs were recorded by stimulating at 30% maximal field amplitude for 10 min prior to beginning experiments (single stimulation every 10 s (0.1 Hz)). The same intensity of stimulation was kept for the remainder of the experiment. After a 10 min stable baseline period, long-term potentiation (LTP) was induced by the following stimulation protocol: 3 trains of 100 stimulations at 100 Hz at the same stimulus intensity, with a 20 s interval between trains. Following this conditioning stimulus, a 1 h test period was recorded where responses were again elicited by a single stimulation every 10 s (0.1 Hz) at the same stimulus intensity. Signals were amplified with an Axopatch 200B amplifier (Molecular Devices, Union City, CA) digitized by a Digidata 1550 interface (Axon Instruments, Molecular Devices, US) and sampled at 10 kHz. Recordings were acquired using Clampex (Molecular Devices) and analyzed with Clampfit (Molecular Devices). Experimenters were blinded to treatment for all experiments.

RESULTS

Screening for miRNAs modulating APP metabolism

We used an unbiased screening approach to identify miRNAs that modulate APP metabolism in our HCS system (Chapuis et al. 2017). Specifically, this model is based on HEK293 cells stably over-expressing an APP fusion protein (mCherry-APP^{695WT}-YFP) that allows for the quantification of intracellular APP fragments. We screened a total of 2,555 mature human miRNAs in a 384-well plate format. As positive control, a siRNA directed against APP was used to calculate the standardized mean difference (denoted as β in **Supplementary Fig. 1**). The complete screen was performed in triplicate and plates with $\beta > 3$ were analyzed according to HCS guidelines (Bray et al. 2013). This procedure led us to identify 50 miRNAs (top and bottom 1%) with the strongest impact on APP metabolism (**Fig. 1a, Supplementary Fig. 1 and Table 1**). Pathway enrichment analysis revealed that these 50 candidate miRNAs are predicted to regulate pathways already identified to involve APP, such as axon guidance (Sosa et al. 2013) and glutamatergic synapse (Martinsson et al. 2019).

To determine which genes were potentially regulated by these top 50 hits, we selected the intersection of predictions resulting from at least four different algorithms (see methods) and thus identified 6,009 putative miRNA-target genes. To further refine the list of predicted genes, we cross-checked them against the 832 genes identified to have a major impact on APP metabolism in our previous genome-wide siRNA screen (**Fig. 1c**). This resulted in 180 common genes that are putative targets of 41 miRNAs.

To determine if any of these 180 genes were preferentially regulated by this pool of 41 miRNAs, we performed 1 million drawing lots of 41 miRNAs among the 2,555 tested and compared them against the list of miRNAs predicted to bind in the 3'-UTR of each of the 180 genes (see **Supplementary Fig. 2**). Distribution of the obtained *p*-values is shown in **Fig. 1d**. *FERMT2* (encoding Kindlin-2), an AD genetic risk factor, was among the 7 most significant genes (*p*-value $< 2.7 \times 10^{-4}$ after Bonferroni correction, **Fig. 1e**), i.e., genes that strongly modulate APP metabolism and whose expression are potentially regulated by miRNAs that also strongly modulate APP metabolism. We therefore focused on this gene.

Endogenous *FERMT2* expression is down-regulated by miRNAs

Four (out of 41) miRNAs were predicted to target *FERMT2* 3'UTR: miR-582-5p, miR-200b-3p, miR-221-3p and miR-222-3p. Of note, we previously identified a variant (rs7143400) within the 3'-UTR of *FERMT2*, where the minor T allele creates an 8-mer binding site for miR-4504 (Delay et al. 2016) (**Fig. 2a and Supplementary Fig. 3**). However, miR-4504 had limited effects on APP metabolism in our HCS (mCherry fold change = 1.18 ± 0.09 , rank 688 in the top 30%). Since the potential effects of this miRNA on *FERMT2* expression would depend on the presence of the rs7143400 minor T allele, we genotyped the HEK293 cell line (used in our HCS) for this variant. We observed that this cell line was homozygous (GG) for rs7143400 and, as a consequence, *FERMT2* expression in this cell line

could not be modulated by miR-4504, potentially limiting its impact on APP metabolism. However, since rs7143400 exhibited genome-wide significance in its association with AD risk, we decided (i) to add miR-4504 to the list of four miRNAs resulting from the HCS screening and (ii) to consider the rs7143400 variant in our subsequent analyses.

We first developed a luciferase activity assay in HEK293 cells to determine if the 5 miRNAs of interest could indeed modulate *FERMT2* expression. The capacity of each miRNA to induce a down-regulation of the reporter gene expression (luciferase activity) in the presence of *FERMT2* 3'UTR sequence was confirmed (**Fig. 2b**). As hypothesized, miR-4504 was able to down-regulate reporter gene expression only in the presence of the rs7143400 T allele. We then assessed whether these miRNAs were also able to modulate endogenous *FERMT2*. For this purpose, we transfected the 5 selected miRNAs in either wild-type HEK293 (HEK293^{WT}) or rs7143400-mutated HEK293 cell lines (HEK293^{rs7143400-G/T}) generated via the Crispr-Cas9 technology (**Supplementary Fig. 4**). All 5 miRNAs were able to decrease the endogenous *FERMT2* expression; however, miR-4504 only in the HEK293^{rs7143400-G/T} cell line (**Fig. 2c and 2d**). Notably, all 5 miRNAs could down-regulate endogenous *FERMT2* expression in HeLa cells that are heterozygous for rs7143400 (**Fig. 2e**).

Collectively, these data suggest that endogenous *FERMT2* expression is dependent on miRNAs expression and that a functional variant is able to modulate the miRNA-dependent *FERMT2* expression by creating a binding site for miRNAs.

APP metabolism is regulated by miRNAs

According to our hypothesis, the 5 miRNAs are potential candidates to modulate APP metabolism through a direct down-regulation of *FERMT2*. However, it is also possible that these miRNAs modulate the APP metabolism through targeting additional genes, making it difficult to determine the true effect of *FERMT2* on the read-outs observed. To assess this question, we reasoned that if a candidate miRNA affects the APP metabolism mainly through down-regulating *FERMT2*, this candidate miRNA would have similar effects on APP metabolism as the direct *FERMT2* down-regulation by siRNAs we assessed previously (Chapuis et al. 2017). For this purpose, we evaluated the effects of miR-582-5p, miR-200b-3p, miR-221-3p and miR-222-3p over-expression on the APP metabolism in HEK293^{WT} cells. Only miR-222-3p was associated with an increase in endogenous APP levels (**Fig. 3a**). We further assessed the impact of miR-222-3p on A β secretion by co-transfecting this miRNA with APP cDNA in HEK293^{WT}. Results showed that miR-222-3p decreased *FERMT2* expression and increased A β secretion in a dose-dependent manner (**Fig. 3b**). Of note, miR-582-5p and miR-200b-3p were also predicted to directly target APP, thus making it impossible to assess whether these miRNAs affected APP metabolism directly or through *FERMT2*.

We also addressed the same question for miR-4504 by taking advantage of the HEK293^{rs7143400-G/T} and HeLa cell lines. As for miR-222-3p, we observed that miR-4504 transfection was associated with an increase in total APP in both cell lines (**Fig. 3c**). Nonetheless, our findings indicate that miR-222-3p

and miR-4504 have the same impact on APP metabolism as seen by FERMT2 silencing alone. To note, the impact of miR-4504 was only observed in HEK293^{rs7143400-G/T} cells.

miR-4504 is over-expressed in AD brains

To provide further physiological relevance to our findings, we combined classical immunocytochemistry with RNA hybridisation allowing miRNAs detection at single-copy sensitivity. We first observed that both miR-222-3p and miR-4504 were expressed in primary hippocampal neurons (**Fig. 4a**). We next measured the expression levels of miR-222-3p and miR-4504 in the post-mortem brain samples from AD patients and control subjects. We observed that the expression levels of miR-4504, but not of miR-222-3p, were significantly increased in AD brains compared to controls (**Fig. 4b**). Taken together, these data suggest that several miRNAs (some of which are over-expressed in AD brains) are able to down-regulate endogenous FERMT2 expression and modulate APP metabolism. In addition, this miRNA-dependent regulation is modulated by a functional genetic variant associated with an increased AD risk in GWAS. This implies that under-expression of FERMT2 is potentially deleterious in an AD pathophysiological context in neurons.

Interaction between FERMT2 and APP controls APP metabolism

How FERMT2 modulates APP metabolism is not fully established. To address this, we tested the possibility that APP and FERMT2 form a protein-protein complex. This hypothesis is supported by proximity ligation assay (PLA) signals in hippocampal primary neuronal cultures (**Fig. 5a**). We then aimed to validate this complex formation via three complementary approaches: (i) Pull-down of endogenous APP from hippocampal primary neuronal culture extracts co-immunoprecipitated endogenous FERMT2 (**Fig. 5b**). (ii) Over-expression of wild-type FERMT2 (FERMT2^{WT}) was also able to pull-down the recombinant intracellular domain of APP (C100) (**Fig. 5c and d**). (iii) In addition, we generated a Q₆₂₁W₆₂₂AA FERMT2 mutant (FERMT2^{QW}) which was previously shown to abolish the interaction between the FERMT2 F3 domain and the NxTY motif of Integrin-β3 (which is also present within the intracellular domain of APP) (Ma et al. 2008). Remarkably, when over-expressed in HEK293 cells, FERMT2^{QW} was not able to pull-down the recombinant intracellular domain of APP. Cumulatively, these findings support a direct interaction between FERMT2 and APP. Based on the recently solved crystal structure of FERMT2 in complex with the integrin-β3-tail (H. Li et al. 2017), we built a structural model of the FERMT2/APP complex (**Fig. 5e**), supporting our hypothesis that a protein-protein interaction exists between FERMT2 and APP.

We next assessed the biological impact of the FERMT2/APP interaction on APP metabolism. By performing extracellular biotinylation experiments, we observed that FERMT2 over-expression in HEK293-APP^{695wt} cell line decreased the levels of APP at the cell surface, an effect that was abolished by the presence of the QW mutation (**Fig. 5f**). Further, a dominant negative effect of the FERMT2^{QW} mutant was observed: its over-expression impacted APP metabolism similarly to FERMT2 silencing,

i.e., resulting in increased mature APP at the cell surface and increased A β production, as previously reported (Chapuis et al. 2017). Altogether, our data suggest that a FERMT2/APP interaction is necessary for FERMT2 to have an impact on APP metabolism. We decided to further characterize the interaction between FERMT2 and APP at the molecular level and to determine how FERMT2 under-expression may modulate neuronal phenotypes in which APP is known to be involved.

FERMT2/APP interaction is involved in axonal growth

During brain development, APP is enriched in axonal growth cones and acts as a co-receptor for axon guidance and cell migration cues through its interaction with the extracellular matrix (Soldano & Hassan 2014) (Sosa et al. 2013). Interestingly, our pathway analysis highlighted axon guidance as the most enriched pathway (**Fig. 1b**). For this reason, we decided to investigate the potential involvement of FERMT2/APP interaction in axon growth. Using primary neurons cultured in microfluidic devices that fluidically isolate axons from their cell bodies, we first observed the co-localization of endogenous FERMT2 with APP, as well as with PLA spots in axonal growth cones (**Fig. 6a**). These data suggest a potential function of the FERMT2/APP complex in axon growth behavior. We then addressed the impact of FERMT2 silencing on axonal growth cone morphology after transduction with lentiviral vectors expressing either shRNA against FERMT2 (shFERMT2) or a non-targeting shRNA (shNT). Actin staining revealed that FERMT2 under-expression led to a significant decrease in growth cone area (9.13 ± 0.71 vs 12.79 ± 1.10 μm^2) as well as in the angular dispersion of growth cone filopodia (0.67 ± 0.04 vs 0.84 ± 0.02) (**Fig. 6b**). Of note, no significant impact on actin retrograde flow rate was observed (0.166 ± 0.003 vs 0.157 ± 0.002 $\mu\text{m/s}$). These observations suggest a potential impairment of the exploration behavior of the growth cones due to FERMT2 silencing, but not an effect on actin dynamics *per se*. FERMT2 under-expression was also associated with an accumulation of endogenous APP in the growth cones (1.38 ± 0.11 vs 0.85 ± 0.08 , after normalization by the growth cone area).

In order to characterize in-depth the impact of FERMT2 and/or APP expression on axonal growth, we conducted time-lapse microscopy and measured axon growth speed at DIV5 following lentiviral transduction (shNT, shFERMT2, or shAPP) of neurons in microfluidic devices at DIV1. FERMT2 silencing led to 31.7% increase in axon growth speed (**Fig. 6c**). Conversely, APP under-expression led to 16.7% decrease in axon growth speed. Remarkably, silencing of APP was able to fully abolish the effect of FERMT2 under-expression on axon growth speed, suggesting that APP was required for the molecular mechanism by which FERMT2 controls the axon growth speed. In addition, we observed that FERMT2^{QW} mutant over-expression was able to induce 15.9% increase in axon growth speed (**Fig. 6c**). Since over-expression of FERMT2^{WT} did not show any impact, these data also suggested a potential dominant negative effect of the FERMT2^{QW} mutant and further supported the involvement of FERMT2/APP complex in axonal growth.

FERMT2 expression regulates synaptic plasticity in APP dependent manner

Next, we decided to investigate the impact of FERMT2 silencing on neuronal maturation at DIV14. First, co-staining between FERMT2 and synaptic markers (Synaptophysin and Homer) suggested the localization of FERMT2 at the synapse (**Fig. 7a**). The presence of FERMT2 in both pre- and postsynaptic compartments was confirmed by synaptosomal purification (**Fig. 7b**). PLA-FERMT2/APP signals were also co-localized with Synaptophysin and Homer puncta (**Fig. 7c**) supporting the possibility of the involvement of FERMT2/APP complex in synapses.

We sought to establish the functional impact of FERMT2 and/or APP silencing on CA1 basal synaptic transmission and long-term potentiation (LTP) in *ex vivo* mouse hippocampal slices, after stereotactic lentivirus injection allowing expression of shNT, shFERMT2, shAPP or shFERMT2+shAPP. No significant difference was observed for the normalized average slope of the evoked field excitatory postsynaptic potential (fEPSP), indicating no alteration of the CA1 basal synaptic transmission in each group analyzed (**Fig. 7d**, **Supplementary Fig. 5**). Then, in the same slice, tetanic stimulation was delivered to the Shaffer collaterals (SC) in order to induce LTP (**Fig. 7e**). Tetanic stimulation of the SC resulted in a robust, long-lasting potentiation of the fEPSP slope in slices from mice infected with shNT and in shAPP, whereas LTP was impaired in slice from shFERMT2-infected mice. An LTP deficit was observed in hippocampal slices infected with shFERMT2, but not in those also infected with shAPP (**Fig. 7e 7f and 7g**). Remarkably, this deficit was abolished when both APP and FERMT2 were silenced, suggesting that APP was required for the molecular mechanism by which FERMT2 impacts LTP.

Discussion

As in other multifactorial diseases, GWAS in AD are agnostic approaches, and how a genetic risk factor is implicated in pathophysiological processes is typically unknown. Sometimes, even the physiological functions of an AD genetic risk factor in the brain are not known. Understanding the role of these genes is thus a challenge that requires several key questions to be addressed: (i) Does the corresponding protein interact with other key players and pathways known to be involved in AD? (ii) What is (are) the functional variant(s) responsible for the GWAS signal and does this (do these) variant(s) impact the biological function of the corresponding protein and its interaction with key players of AD? (iii) How does the protein (taking into account how the functional variant(s) impact the protein) modulate the physiological and/or pathophysiological functions of key players/pathways?

With these questions in mind, we developed systematic approaches to determine the genes that are involved in APP metabolism, a major player in AD development. To this end, we previously developed an HCS, based on the quantification of intracellular APP fragments, to measure the impact of under-expression of 18,107 genes (*via* siRNA pools) on APP metabolism (Chapuis et al. 2017). In the current study, we screened the impact of the over-expression of 2,555 miRNAs on APP metabolism with the hypothesis that genes (i) that modulate APP metabolism (ii) whose expression

levels are regulated by miRNAs that also modulate the APP metabolism are likely some of the key actors controlling APP metabolism and functions. The convergence of these two agnostic screens highlighted FERMT2, a GWAS-defined genetic risk factor of AD, for which almost nothing is known in the cerebral and AD contexts. We thus proposed that FERMT2 could be down-regulated by several miRNAs and involved in AD through regulating APP metabolism and/or function (**Fig. 8**).

Of note, we previously identified the rs7143400 variant located in FERMT2 3'UTR as susceptible to alter a binding site for miR-4504 (Delay et al. 2016). Here, in addition to *in silico* prediction supporting the impact of this variant on miRNA binding (**Supplementary Fig. 3**), we demonstrate that this variant is functional: the AD-associated rs7143400 T allele down-regulates *FERMT2* and modulates APP metabolism via its interaction with miR-4504. Remarkably, we observed that miR-4504 is over-expressed in the brains of AD cases compared to controls, and is mainly expressed in neurons in primary mixed hippocampal cultures.

Together, our data indicate that a deleterious over-expression of miR-4504 can lead to a decrease in FERMT2 expression in individuals bearing the rs7143400 minor T allele, which subsequently modulates APP metabolism (**Fig. 8**). Supporting a link between FERMT2 and APP metabolism, studies from cohorts of patients have reported an association between variants in *FERMT2* gene and A β in CSF (Chapuis et al. 2017) and brain amyloidosis (Apostolova et al. 2018).

Of note, in publicly-available RNA-seq analyses (Mayo Clinic Brain Bank), an over-expression of FERMT2 mRNA is observed in post-mortem human temporal cortex of AD patients relative to controls (Sullivan et al. 2018). Even if we did not observe such a variation of the FERMT2 mRNA level in a smaller number of brains, we nevertheless detected an increase in the protein levels as a function of Braak stages, especially at the latter stages (**Supplementary Fig. 6**). This point is of particular importance since in the Genotype-Tissue Expression Database (GTEx Consortium et al. 2015), FERMT2 variants associated with an increase in AD risk at the genome-wide significance level are also part of an expression quantitative trait locus, significantly associated with decreased brain expression of FERMT2 mRNA (sentinel variant in GWAS rs17125924; -18% p -value = 2×10^{-6}). This observation strongly supports our conclusion that FERMT2 under-expression is deleterious and suggests that FERMT2 down-regulation would be deleterious at the earliest stage of the disease, whereas, FERMT2 over-expression may occur as a pathological consequence at a very late stage. Here, we propose that FERMT2 down-regulation at the earliest stage of AD would depend in part on (i) the miR-4504 expression, (ii) cerebral cell type (i.e., neurons), and (iii) the presence of the rs7143400 minor T allele (observed in 9% of Caucasians). Unfortunately, it is important to keep in mind that all these constraints will make difficult, if not impossible, to detect such a miRNA-dependent decrease in FERMT2 mRNA levels. Of note, this point may also underline the limitation of expression databases in deciphering the mechanisms underlying the functional effects of GWAS variants, for they do not allow capturing (even hide) subtle mechanisms.

Our current hypothesis holds that FERMT2 controls APP internalization and degradation (Chapuis et al. 2017), such that FERMT2 silencing leads to a greater amount of full-length APP and by-products and FERMT2 over-expression leads to a reduction of these metabolites. In the current paper, we demonstrate that a direct interaction between FERMT2 and APP –through the F3 domain of FERMT2 and the NxTY motif within APP’s intracellular domain– is necessary for FERMT2 to have an impact on APP metabolism. Moreover, we observed that the FERMT2/APP interaction could be involved in the regulation of axonal growth in line with APP’s function within the growth cone (Sosa et al. 2013) (data we replicated in this study). Because APP silencing abolishes the impact of FERMT2 silencing on axon growth speed, we could postulate that the effect of FERMT2 might be –at least in part– due to the accumulation of full-length APP or its by-products within the growth cone, impairing vesicle trafficking and/or cell adhesion.

Apart from this developmental read-out, we also analyzed synaptic plasticity, a read-out more relevant to AD, where synaptic dysfunction/loss is one of the earliest events observed. FERMT2 under-expression leads to a harmful effect on LTP in an APP-dependent manner. As FERMT2 silencing leads to an accumulation of full-length APP and all by-products (including A β peptides), we can hypothesize that these accumulations could be involved in the synaptic dysfunction observed when FERMT2 is under-expressed. Moreover, it could explain why APP expression seems to be required (for FERMT2 to impact developmental and synaptic read-outs), although further experiments are needed to decipher the consequences of the causal link between FERMT2 and APP, i.e., to determine whether it impacts full-length APP function or invokes A β synaptotoxicity.

This is of particular interest since, APP shedding strongly enhances its cell adhesion and synaptogenic activity (Stahl et al. 2014). Moreover, the APP intracellular domain is required for normal synaptic morphology and synaptic plasticity, suggesting that intracellular interactors could be required for proper synaptic function (Klevanski et al. 2015). Remarkably, we have recently proposed a circular model of AD pathogenesis, where the core of the focal adhesion pathway –which FERMT2 and APP are part of– may participate in the dysfunction of synaptic plasticity in AD (Dourlen et al. 2019).

In conclusion, we propose that FERMT2 under-expression through miRNAs and/or genetic regulation leads to synaptic dysfunction in an APP-dependent manner. Our hypothesis may thus call for new therapeutic approaches in AD targeting FERMT2 and/or APP function, rather than A β peptide production/clearance. Once therapeutic approaches that target FERMT2-dependent pathways are eventually developed, one can argue that it might be an example of personalized medicine for AD, preferentially targeting patients who have high levels of miR-4504 and who bear the rs7143400 minor T allele.

Acknowledgements

F. E. benefited from a doctoral grant co-funded by Hauts-de-France Regional Council and Institut Pasteur de Lille. The authors thank the BICeL and EquipEx ImagInEx HCS platforms of the Institut Pasteur de Lille and Alexandre Vandeputte for technical assistance. The authors thank Karine Blary at the IEMN Lille for the microfabrication work. This work was partly supported by the French RENATECH network. This study was funded by INSERM, Institut Pasteur de Lille, the Centres of Excellence in Neurodegeneration-ANR program (CoEN, GWAS in AD: focus on microRNA), the Canadian Institute of Health Research (CHIR), la Fondation Alzheimer (Syn-Alz), the EU Joint Programme – Neurodegenerative Diseases Research (JPND; 3DMiniBrain) and Fondation Vaincre Alzheimer (FR-17006p). This work was also funded by the Lille Métropole Communauté Urbaine and the French government's LABEX DISTALZ program (development of innovative strategies for a transdisciplinary approach to Alzheimer's disease). This work was supported for M.H by Academy of Finland (grant number 307866); Sigrid Jusélius Foundation; the Strategic Neuroscience Funding of the University of Eastern Finland. The authors thank the vectorology platform Transbiomed for lentivirus production.

Author contributions

J.-C. L. and J. C. designed and supervised research. A.F., F.E., F.C and C.B. performed APP metabolism and FERMT2/APP interaction analyses. X. H. developed in silico model for FERMT2/APP interaction. F. E. and D. K. performed and analyzed axon growth experiments. A. C., A. F., J. D. and J. C. developed Crispr/Cas9 model and/or performed subsequent analyses. C. D., A.-C. V., A. F. and B. G.-B. designed and/or performed miRNA screening and/or statistical analyses. S. H. and M. F. performed and analyzed electrophysiology experiments. A. F., T. M., F. D. and S. D. performed primary neuronal cultures. M. M., M. T., I. P. and M. H. analyzed transcriptomic and/or proteomic data of FERMT2 expression in brains. E. B. and S. S. H. performed miR expression quantification in brains. F. E., N. M., D. K. and J. C. participated in image acquisition and analyses of APP/FERMT2 interaction and/or synapse density. F. E., P. A., J. D., D. K., J.-C. L. and J. C. wrote and/or revised the paper.

Conflicts of interest

S. H. and M. F. are full-time employees of E-Phy-Science SA. C. D. has been an employee of Janssen Pharmaceutica since her departure from the laboratory Inserm U1167 in 2016.

References

- Agarwal, V. et al., 2015. Predicting effective microRNA target sites in mammalian mRNAs. *eLife*, 4. Available at: <https://elifesciences.org/articles/05005> [Accessed September 2, 2019].
- Apostolova, L.G. et al., 2018. Associations of the Top 20 Alzheimer Disease Risk Variants With Brain Amyloidosis. *JAMA Neurology*, 75(3), p.328. Available at: <http://www.ncbi.nlm.nih.gov/pubmed/29340569> [Accessed April 27, 2018].
- Bandyopadhyay, S. & Mitra, R., 2009. TargetMiner: microRNA target prediction with systematic identification of tissue-specific negative examples. *Bioinformatics (Oxford, England)*, 25(20), pp.2625–31. Available at: <https://academic.oup.com/bioinformatics/article-lookup/doi/10.1093/bioinformatics/btp503> [Accessed September 2, 2019].
- Blasiak, A., Lee, G.U. & Kilinc, D., 2015. Neuron Subpopulations with Different Elongation Rates and DCC Dynamics Exhibit Distinct Responses to Isolated Netrin-1 Treatment. *ACS chemical neuroscience*, 6(9), pp.1578–90. Available at: <http://pubs.acs.org/doi/10.1021/acschemneuro.5b00142> [Accessed September 11, 2019].
- Bray, M.-A., Carpenter, A. & Imaging Platform, B.I. of M. and H., 2013. *Advanced Assay Development Guidelines for Image-Based High Content Screening and Analysis*, Eli Lilly & Company and the National Center for Advancing Translational Sciences. Available at: <http://www.ncbi.nlm.nih.gov/pubmed/23469374> [Accessed July 13, 2016].
- Chapuis, J. et al., 2017. Genome-wide, high-content siRNA screening identifies the Alzheimer's genetic risk factor FERMT2 as a major modulator of APP metabolism. *Acta Neuropathologica*, 133(6), pp.955–966. Available at: <http://www.ncbi.nlm.nih.gov/pubmed/27933404> [Accessed August 19, 2019].
- Checler, F., 1995. Processing of the beta-amyloid precursor protein and its regulation in Alzheimer's disease. *Journal of neurochemistry*, 65(4), pp.1431–44. Available at: <http://www.ncbi.nlm.nih.gov/pubmed/7561836> [Accessed July 13, 2016].
- Delay, C. et al., 2016. miRNA-dependent target regulation: functional characterization of single-nucleotide polymorphisms identified in genome-wide association studies of Alzheimer's disease. *Alzheimer's research & therapy*, 8(1), p.20. Available at: <http://www.ncbi.nlm.nih.gov/pubmed/27215977> [Accessed June 17, 2016].
- Delay, C., Mandemakers, W. & Hébert, S.S., 2012. MicroRNAs in Alzheimer's disease. *Neurobiology of disease*, 46(2), pp.285–90. Available at: <https://linkinghub.elsevier.com/retrieve/pii/S0969996112000186> [Accessed August 19, 2019].
- Dourlen, P. et al., 2019. The new genetic landscape of Alzheimer's disease: from amyloid cascade to genetically driven synaptic failure hypothesis? *Acta neuropathologica*, 138(2), pp.221–236. Available at: <http://link.springer.com/10.1007/s00401-019-02004-0> [Accessed August 23, 2019].
- Frandemiche, M.L. et al., 2014. Activity-dependent tau protein translocation to excitatory synapse is disrupted by exposure to amyloid-Beta oligomers. *The Journal of neuroscience : the official journal of the Society for Neuroscience*, 34(17), pp.6084–97. Available at: <http://www.ncbi.nlm.nih.gov/pubmed/24760868> [Accessed April 29, 2014].
- GTEx Consortium, K.G. et al., 2015. Human genomics. The Genotype-Tissue Expression (GTEx) pilot analysis: multitissue gene regulation in humans. *Science (New York, N.Y.)*, 348(6235),

- pp.648–60. Available at: <http://www.sciencemag.org/cgi/doi/10.1126/science.1262110> [Accessed September 3, 2019].
- Hardy, J., 1997. Amyloid, the presenilins and Alzheimer's disease. *Trends in neurosciences*, 20(4), pp.154–9. Available at: <http://www.ncbi.nlm.nih.gov/pubmed/9106355> [Accessed November 2, 2016].
- Hardy, J. & Selkoe, D.J., 2002. The amyloid hypothesis of Alzheimer's disease: progress and problems on the road to therapeutics. *Science.*, %19;297(5580), pp.353–356.
- Hébert, S.S. et al., 2008. Loss of microRNA cluster miR-29a/b-1 in sporadic Alzheimer's disease correlates with increased BACE1/beta-secretase expression. *Proceedings of the National Academy of Sciences of the United States of America*, 105(17), pp.6415–20. Available at: <http://www.pnas.org/cgi/doi/10.1073/pnas.0710263105> [Accessed August 19, 2019].
- Hsu, S.-D. et al., 2011. miRTarBase: a database curates experimentally validated microRNA–target interactions. *Nucleic Acids Research*, 39(suppl_1), pp.D163–D169. Available at: <https://academic.oup.com/nar/article-lookup/doi/10.1093/nar/gkq1107> [Accessed September 2, 2019].
- Jansen, I.E. et al., 2019. Genome-wide meta-analysis identifies new loci and functional pathways influencing Alzheimer's disease risk. *Nature Genetics*, 51(3), pp.404–413. Available at: <http://www.ncbi.nlm.nih.gov/pubmed/30617256> [Accessed September 4, 2019].
- John, B. et al., 2004. Human MicroRNA targets. James C. Carrington, ed. *PLoS biology*, 2(11), p.e363. Available at: <https://dx.plos.org/10.1371/journal.pbio.0020363> [Accessed September 2, 2019].
- Jonsson, T. et al., 2012. A mutation in APP protects against Alzheimer's disease and age-related cognitive decline. *Nature*, 488(7409), pp.96–99. Available at: <http://www.nature.com/doi/10.1038/nature11283>.
- Kaech, S. & Banker, G., 2006. Culturing hippocampal neurons. *Nature protocols*, 1(5), pp.2406–15. Available at: <http://www.nature.com/articles/nprot.2006.356> [Accessed September 19, 2019].
- Kim, M. et al., 2009. Potential late-onset Alzheimer's disease-associated mutations in the ADAM10 gene attenuate {alpha}-secretase activity. *Human molecular genetics*, 18(20), pp.3987–96. Available at: <https://academic.oup.com/hmg/article-lookup/doi/10.1093/hmg/ddp323> [Accessed September 4, 2019].
- Klevanski, M. et al., 2015. The APP Intracellular Domain Is Required for Normal Synaptic Morphology, Synaptic Plasticity, and Hippocampus-Dependent Behavior. *Journal of Neuroscience*, 35(49), pp.16018–16033. Available at: <http://www.ncbi.nlm.nih.gov/pubmed/26658856> [Accessed January 31, 2017].
- Kunkle, B.W. et al., 2019. Genetic meta-analysis of diagnosed Alzheimer's disease identifies new risk loci and implicates A β , tau, immunity and lipid processing. *Nature Genetics*, 51(3), pp.414–430. Available at: <http://www.ncbi.nlm.nih.gov/pubmed/30820047> [Accessed July 12, 2019].
- Li, H. et al., 2017. Structural basis of kindlin-mediated integrin recognition and activation. *Proceedings of the National Academy of Sciences of the United States of America*. Available at: <http://www.ncbi.nlm.nih.gov/pubmed/28739949> [Accessed July 31, 2017].

- Li, Z. et al., 2017. Long non-coding RNA ATB promotes malignancy of esophageal squamous cell carcinoma by regulating miR-200b/Kindlin-2 axis. *Cell Death and Disease*, 8(6), p.e2888. Available at: <http://www.ncbi.nlm.nih.gov/pubmed/28640252> [Accessed June 26, 2017].
- Long, J.M. et al., 2019. Novel upregulation of amyloid- β precursor protein (APP) by microRNA-346 via targeting of APP mRNA 5'-untranslated region: Implications in Alzheimer's disease. *Molecular Psychiatry*, 24(3), pp.345–363. Available at: <http://www.nature.com/articles/s41380-018-0266-3> [Accessed September 3, 2019].
- Ma, Y.-Q. et al., 2008. Kindlin-2 (Mig-2): a co-activator of beta3 integrins. *The Journal of cell biology*, 181(3), pp.439–46. Available at: <http://www.pubmedcentral.nih.gov/articlerender.fcgi?artid=2364684&tool=pmcentrez&rendertype=abstract> [Accessed October 15, 2014].
- Martinsson, I. et al., 2019. APP depletion alters selective pre- and post-synaptic proteins. *Molecular and Cellular Neuroscience*, 95, pp.86–95. Available at: <http://www.ncbi.nlm.nih.gov/pubmed/30763689> [Accessed September 2, 2019].
- Meijering, E., Dzyubachyk, O. & Smal, I., 2012. Methods for cell and particle tracking. *Methods in enzymology*, 504, pp.183–200. Available at: <https://linkinghub.elsevier.com/retrieve/pii/B9780123918574000094> [Accessed September 11, 2019].
- Miranda, K.C. et al., 2006. A pattern-based method for the identification of MicroRNA binding sites and their corresponding heteroduplexes. *Cell*, 126(6), pp.1203–17. Available at: <https://linkinghub.elsevier.com/retrieve/pii/S0092867406010993> [Accessed September 2, 2019].
- Morris, G.P., Clark, I.A. & Vissel, B., 2018. Questions concerning the role of amyloid- β in the definition, aetiology and diagnosis of Alzheimer's disease. *Acta Neuropathologica*, 136(5), pp.663–689. Available at: <http://www.ncbi.nlm.nih.gov/pubmed/30349969> [Accessed September 4, 2019].
- Paraskevopoulou, M.D. et al., 2013. DIANA-microT web server v5.0: service integration into miRNA functional analysis workflows. *Nucleic Acids Research*, 41(W1), pp.W169–W173. Available at: <http://academic.oup.com/nar/article/41/W1/W169/1100417/DIANAmicroT-web-server-v50-service-integration> [Accessed September 2, 2019].
- Patrick, E. et al., 2017. Dissecting the role of non-coding RNAs in the accumulation of amyloid and tau neuropathologies in Alzheimer's disease. *Molecular neurodegeneration*, 12(1), p.51. Available at: <http://molecularneurodegeneration.biomedcentral.com/articles/10.1186/s13024-017-0191-y> [Accessed September 3, 2019].
- Schratt, G., 2009. microRNAs at the synapse. *Nature Reviews Neuroscience*, 10(12), pp.842–849. Available at: <http://www.nature.com/doi/10.1038/nrn2763> [Accessed August 1, 2017].
- Sevalle, J. et al., 2009. Aminopeptidase A contributes to the N-terminal truncation of amyloid beta-peptide. *Journal of neurochemistry*, 109(1), pp.248–56. Available at: <http://doi.wiley.com/10.1111/j.1471-4159.2009.05950.x> [Accessed October 8, 2019].
- Smith, P.Y. et al., 2011. MicroRNA-132 loss is associated with tau exon 10 inclusion in progressive supranuclear palsy. *Human molecular genetics*, 20(20), pp.4016–24. Available at: <https://academic.oup.com/hmg/article-lookup/doi/10.1093/hmg/ddr330> [Accessed September 2, 2019].

- Soldano, A. & Hassan, B. a., 2014. Beyond pathology: APP, brain development and Alzheimer's disease. *Current Opinion in Neurobiology*, 27, pp.61–67. Available at: <http://dx.doi.org/10.1016/j.conb.2014.02.003>.
- Sosa, L.J. et al., 2013. Amyloid precursor protein is an autonomous growth cone adhesion molecule engaged in contact guidance. *PloS one*, 8(5), p.e64521. Available at: <http://www.pubmedcentral.nih.gov/articlerender.fcgi?artid=3653867&tool=pmcentrez&rendertype=abstract> [Accessed October 24, 2014].
- Stahl, R. et al., 2014. Shedding of APP limits its synaptogenic activity and cell adhesion properties. *Frontiers in cellular neuroscience*, 8, p.410. Available at: <http://www.ncbi.nlm.nih.gov/pubmed/25520622> [Accessed January 11, 2017].
- Sullivan, S.E. et al., 2018. Candidate-based screening via gene modulation in human neurons and astrocytes implicates FERMT2 in A β and TAU proteostasis. *Human Molecular Genetics*. Available at: <https://academic.oup.com/hmg/advance-article/doi/10.1093/hmg/ddy376/5145655> [Accessed October 30, 2018].
- Vlachos, I.S. et al., 2015. DIANA-miRPath v3.0: deciphering microRNA function with experimental support. *Nucleic acids research*, 43(W1), pp.W460–6. Available at: <https://academic.oup.com/nar/article-lookup/doi/10.1093/nar/gkv403> [Accessed September 11, 2019].
- Wong, N. & Wang, X., 2015. miRDB: an online resource for microRNA target prediction and functional annotations. *Nucleic acids research*, 43(Database issue), pp.D146–52. Available at: <http://academic.oup.com/nar/article/43/D1/D146/2437436/miRDB-an-online-resource-for-microRNA-target> [Accessed September 3, 2019].

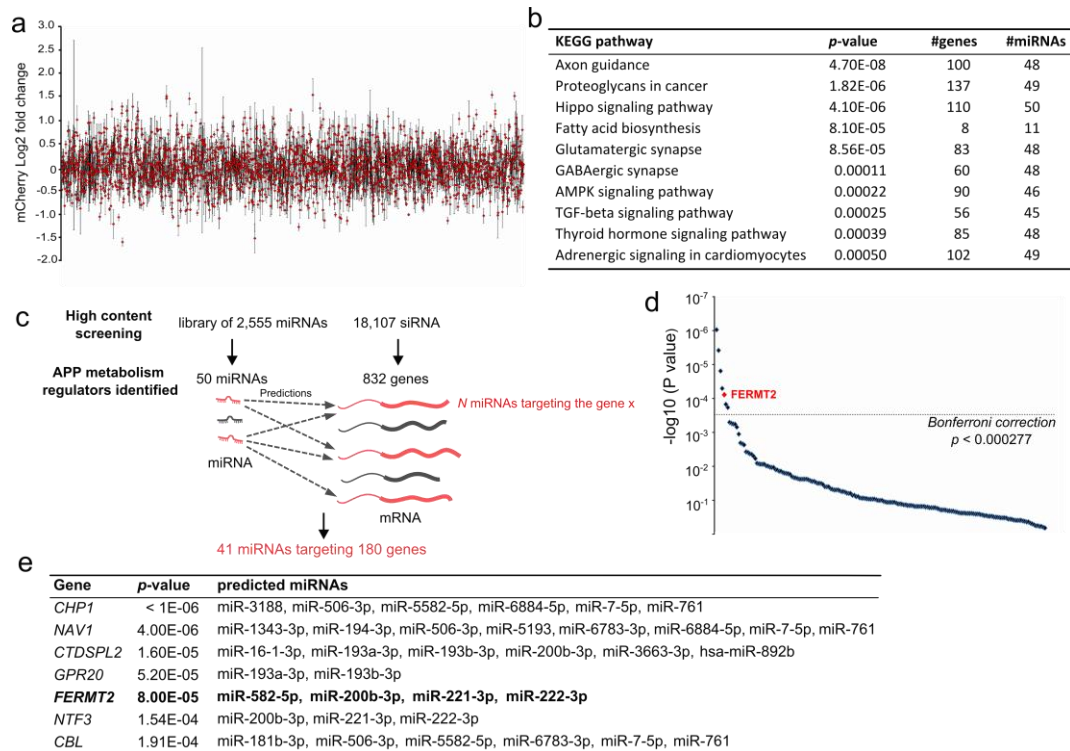


Fig 1. High-content miRNA screening identifies modulators of APP metabolism

a. Mean fluorescence intensity variations (\log_2 fold change) of the mCherry signal obtained during the microRNA (miRNA or miR) screen, conducted in triplicate. The mCherry signal was used to determine the 1% hits exhibiting the strongest variation (0.5% showing an upregulation and 0.5% showing a downregulation). **b.** The 10 most likely canonical pathways identified after pathway enrichment analysis using DIANA Tools mirPath (v3.0). **c.** A graphical representation of the workflow developed to identify miRNA-targeted genes that are also able to modulate APP metabolism according to our genome-wide, high-content siRNA screening. Predictions of target sites for genes expressed in the brain were determined by at least 4 out of 7 software programs used (see methods). **d.** p-value distribution for the 180 genes targeted by the 41 miRNAs identified by HCS (see Fig. S2). **e.** Genes significantly enriched to be targeted by these 41 miRNAs after Bonferroni correction ($0.05/180=2.7 \times 10^{-4}$). Bold text indicates the only AD genetic risk factor in the list and its predicted miRNAs.

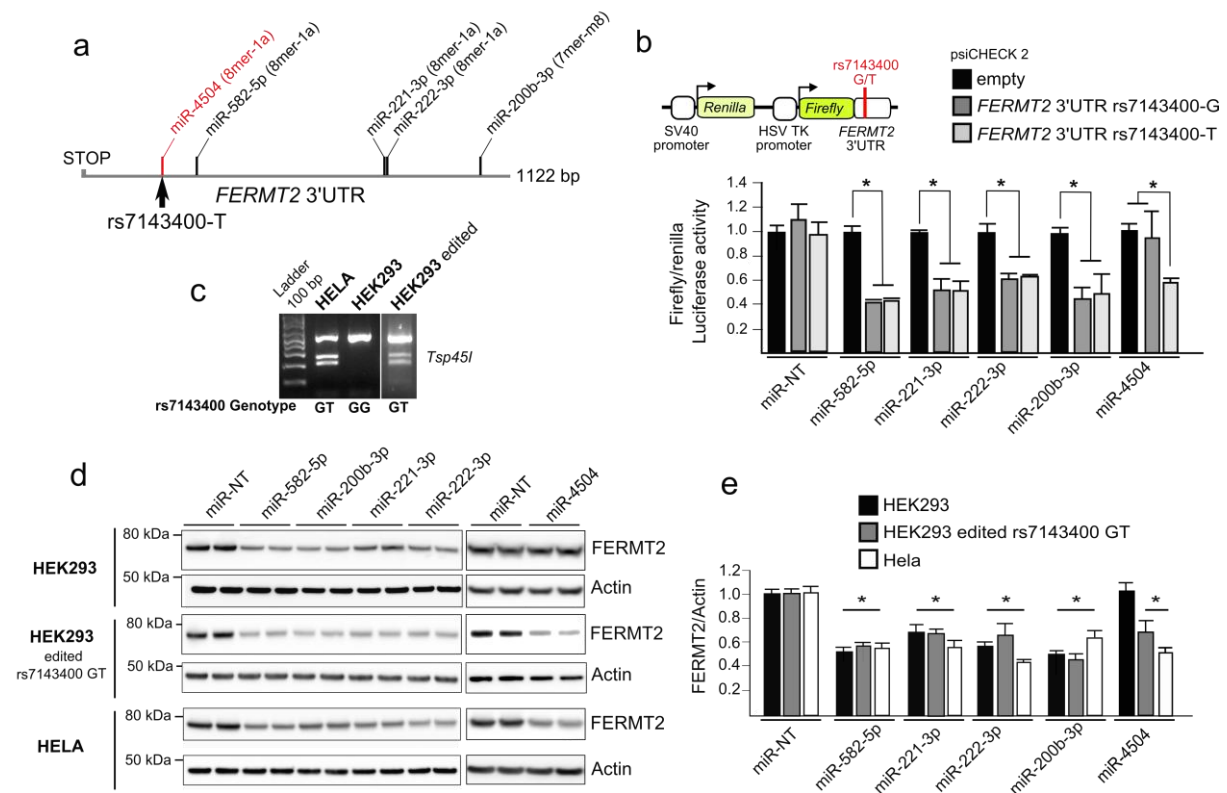


Fig 2. Validation of functional miRNAs targeting *FERMT2* 3'UTR

a. Relative positions of miRNA target sites on *FERMT2* 3'UTR. Target sites created by the rs7143400-T allele, which is associated with AD risk, are shown in red. **b.** Luciferase assay showing the effect of rs7143400-G/T on the repressor activities of 5 miRNAs with regard to the 3'-UTR of *FERMT2* in HEK293 cells. **c.** RFLP genotyping of HeLa and HEK293 cell lines edited or not for the rs7143400 via CRISPR-Cas9 (**supplementary fig. 4**). **d.** Endogenous *FERMT2* expression levels were assessed by Western blot using indicated cell extracts following transient transfection with a non-targeting miR (miR-NT) or with the indicated miR for 72 h. **e.** WB quantifications from three independent experiments as in d. Histograms indicate the mean \pm SD. Mann-Whitney test, * p<0.05.

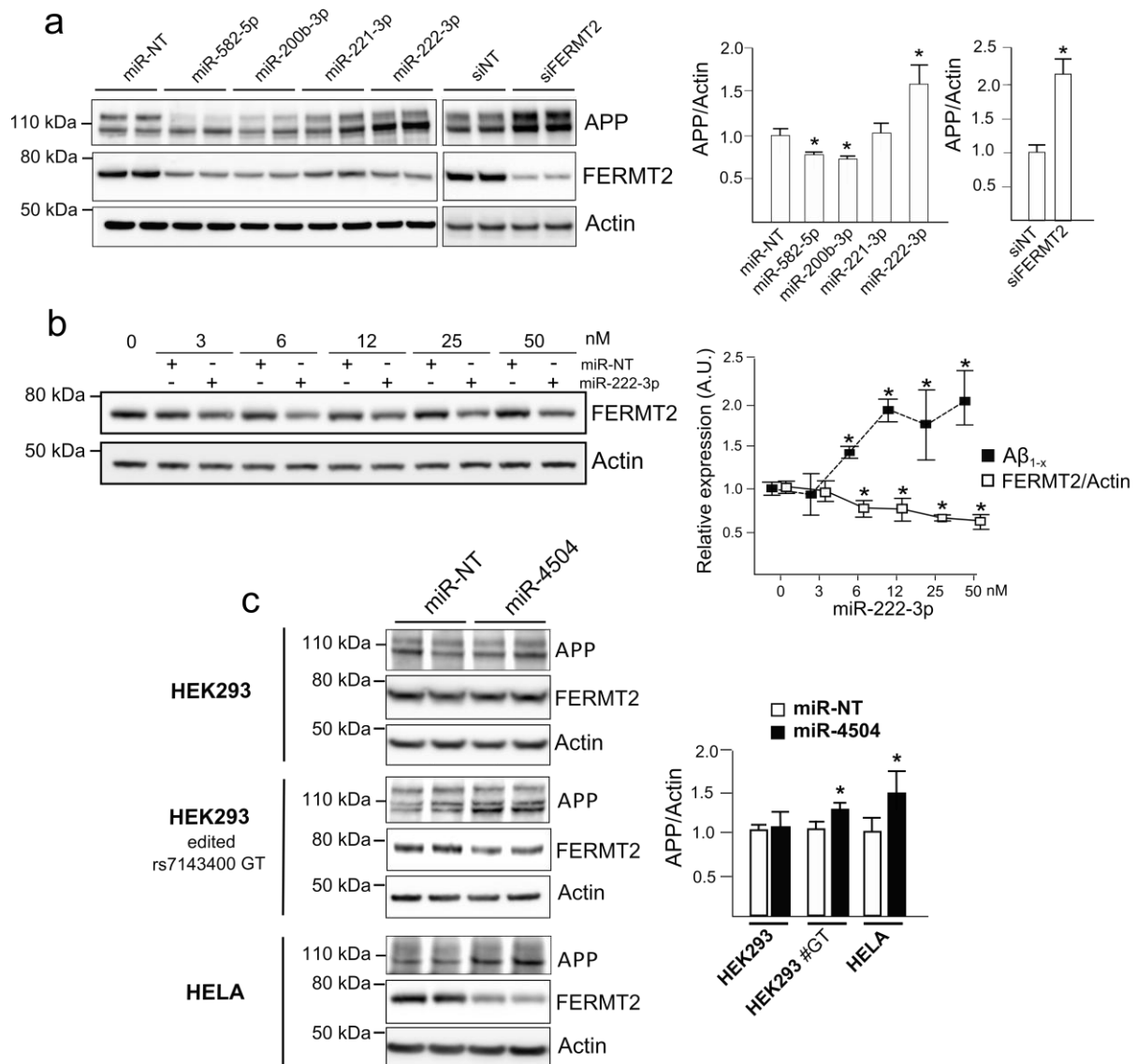


Fig 3. Impact of miRNAs on APP metabolism

a. Endogenous FERMT2 and APP expression levels were assessed by Western blot using HEK293 cell extracts following transient transfection with a non-targeting miR (miR-NT) or with the indicated miR for 72 h. **b.** Endogenous FERMT2 expression levels were assessed by Western blot and $A\beta_{1-x}$ by Alpha-LISA, using HEK293-APP cell extracts following transient transfection with miR-222-3p at the indicated concentration for 72 h. **c.** Endogenous FERMT2 and APP expression levels were assessed by Western blot using cell lines carrying the rs7143400-T allele (or not) following transient transfection with a non-targeting miR (miR-NT) or miR-4504 for 72 h. Histograms indicate the mean \pm SD. A.U., arbitrary units. Mann-Whitney test, * $p < 0.05$.

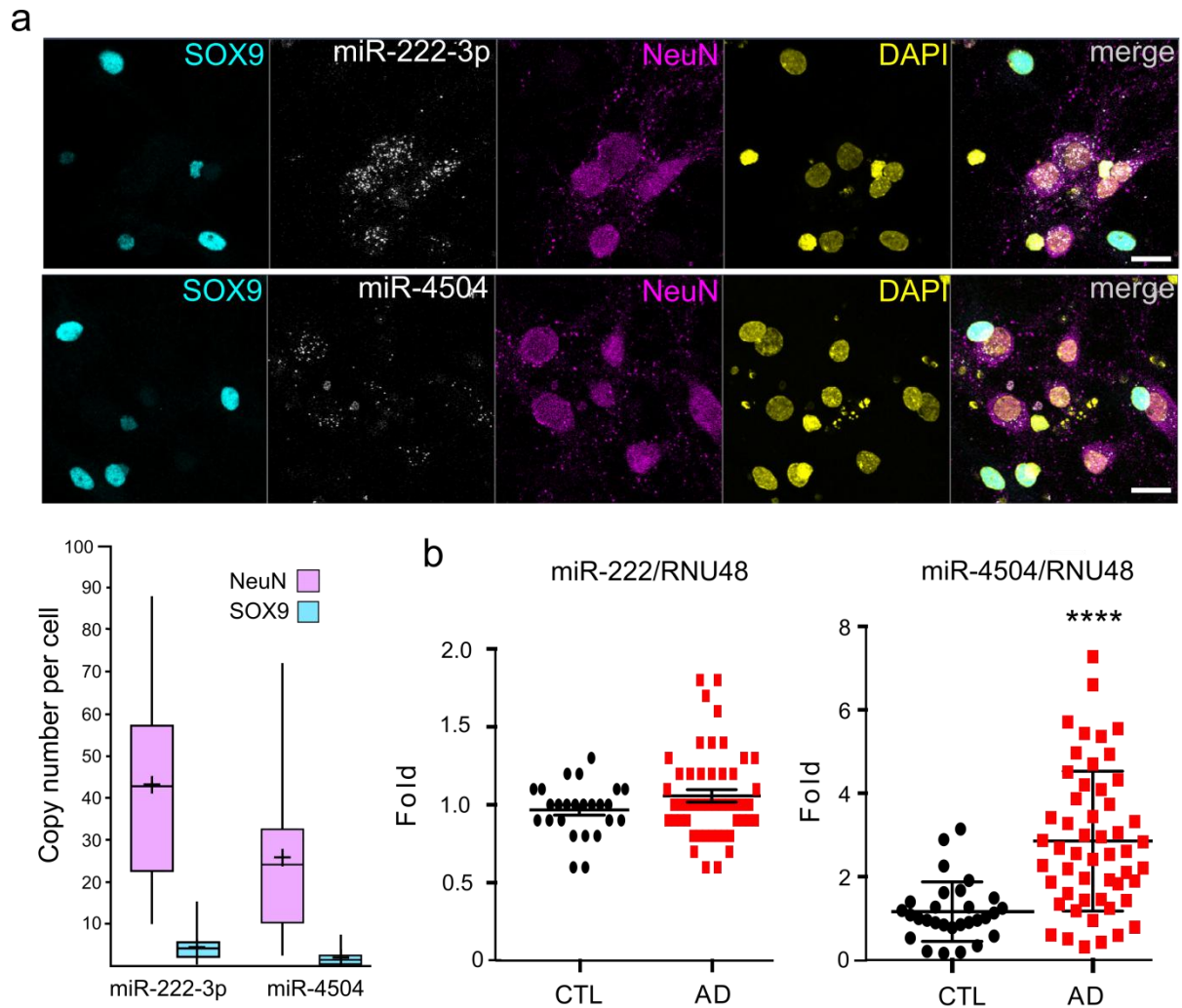


Fig 4. Expression of miRNAs in primary neurons and in AD brains

a. miR-222-3p and miR-4504 are expressed in primary hippocampal neurons. Hybridization experiments in rat postnatal hippocampal neuron cultures enabling single-copy detection of miRNA combined with immunocytochemistry against astrocytic (SOX9) and neuronal (NeuN) markers. Scale bar = 20 μ m. The box plot shows the quantification of miRNA copy number in SOX9- or NeuN-positive cells ($N > 30$ cells for each condition). Cross: mean copy number per cell; middle line: median; upper horizontal line: inclusion of 75%; lower horizontal line: inclusion of 25%. **b.** Expression of miR-4504 is increased in AD brains. Relative miR-222 and miR-4504 expression levels in temporal lobes of non-demented (CTL) and AD groups. Mann–Whitney test; **** $p < 0.0001$.

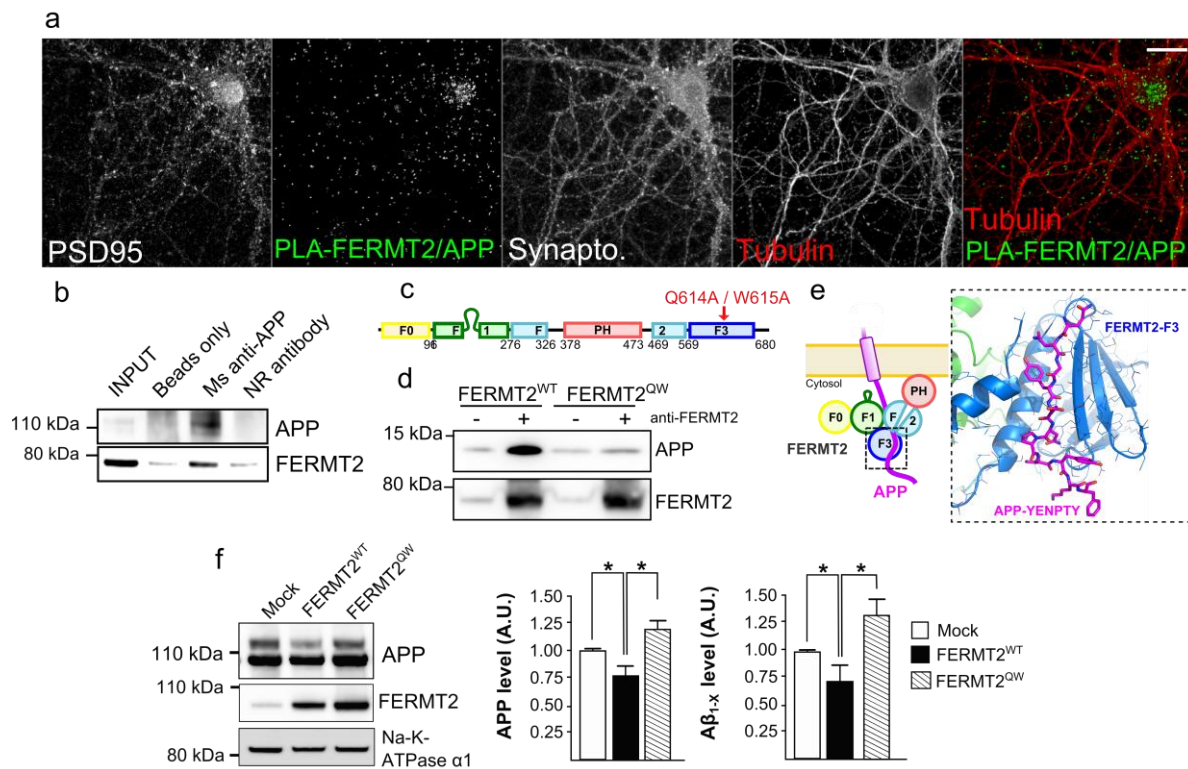


Fig 5. Interaction between FERMT2 and APP controls APP metabolism

a. Localization of proximity ligation assay (PLA) signals between endogenous APP and FERMT2 in hippocampal neurons. PLA was co-stained with antibodies against post- and presynaptic markers (PSD95 and Synaptophysin, respectively) and α -tubulin. Scale bar = 10 μ m. **b.** Co-IP between endogenous APP and FERMT2 from membrane extracts of hippocampal PNC. Protein extracts were incubated with beads only, a mouse (Ms) antibody against APP (4G8) or a non-relevant (NR) antibody. **c.** The domain organization of FERMT2 protein. Q614A/W615A (QW) mutation was reported to abolish the interaction of F3 domain of FERMT2 with the NxTY motif. **d.** APP pull-down experiment with wild type (WT) or mutated (QW) FERMT2. Protein extracts from HeLa cells overexpressing FERMT2^{WT} or FERMT2^{QW} were incubated with recombinant APP C-terminal fragment (C100). **e.** Structural model of the FERMT2-APP complex built by homology using the crystal structure of the FERMT2-Integrin- β 3-tail complex (H. Li et al. 2017). **f.** The impact of FERMT2 on APP metabolism in HEK293-APP^{695WT} cells is reverted with the overexpression of FERMT2^{QW} compared to FERMT2^{WT}.

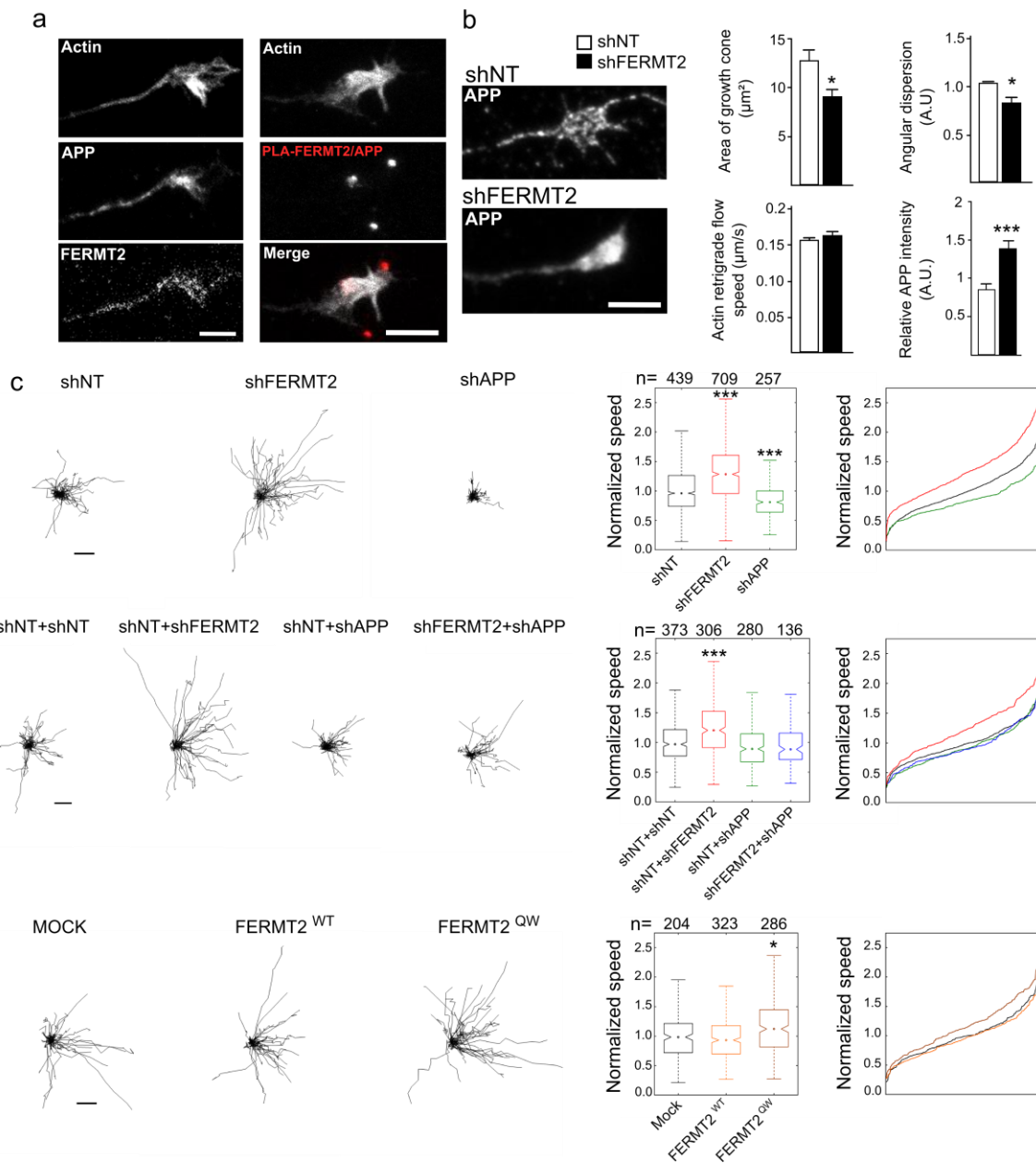


Fig 6. FERMT2/APP complex is involved in axonal growth

a. Immunofluorescence images showing the presence of APP and FERMT2 within the axonal growth cone stained with SiR-actin. The right panel shows the presence of PLA-FERMT2/APP puncta within the axonal growth cone. **b.** Impact of lentiviral transduction of non-targeting shRNA (shNT) or shRNA against FERMT2 (shFERMT2) on the area of the growth cone, angular dispersion and speed of the actin retrograde flow, and APP immunostaining. **c.** Impact of lentiviral transduction on axonal growth speed. Individual axon tracks from a representative set are plotted. Scale bars = 50 μm . Box plots and cumulative distribution plots are color-matched. N is the number of axons analyzed from at least three independent experiments. Kruskal-Wallis ANOVA with multiple comparisons; * $p < 5 \times 10^{-3}$; *** $p < 5 \times 10^{-7}$.

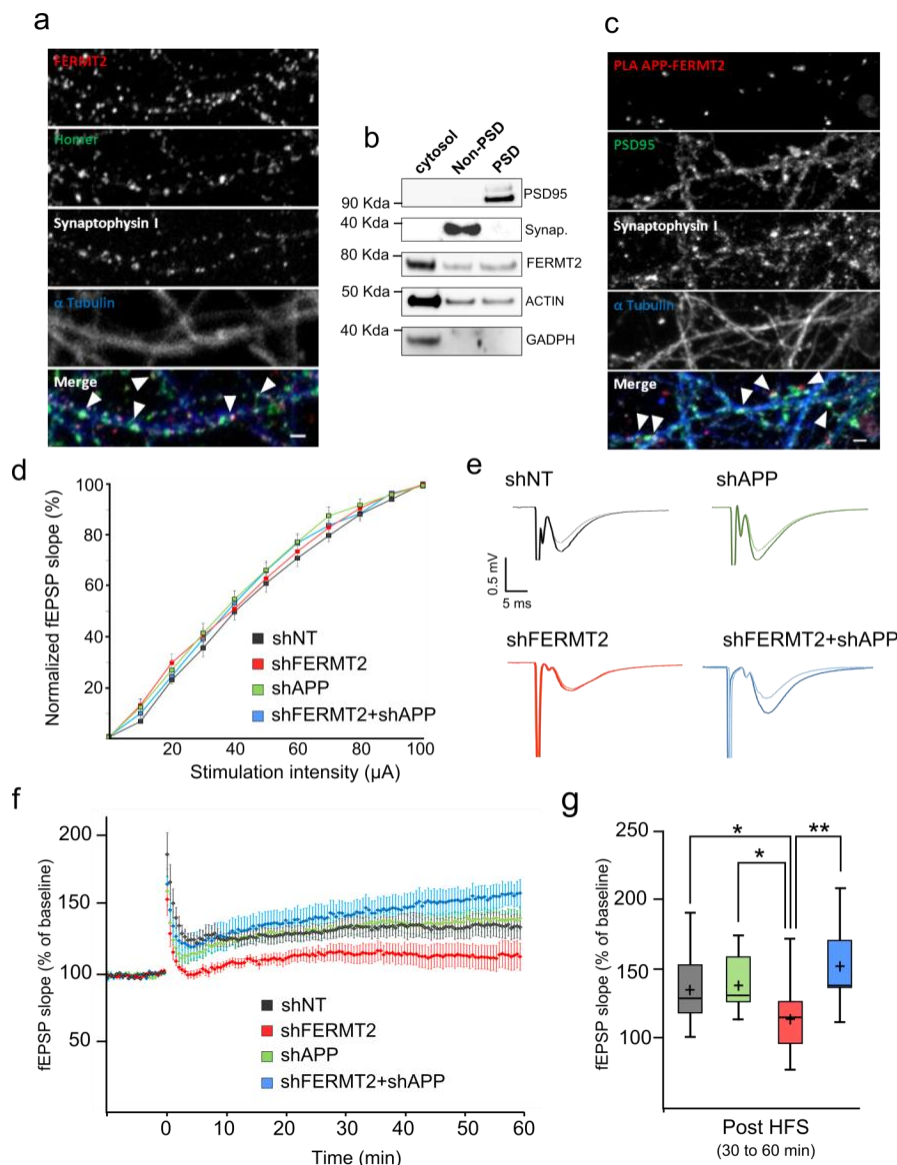


Fig 7. FERMT2 is present at the synapse and modulates synaptic plasticity

a. Immunofluorescence in hippocampal primary neuronal culture showing a co-localization of FERMT2 staining with post- and presynaptic markers (Homer and Synaptophysin, respectively). **b.** Synaptic fractionation experiment revealed the presence of FERMT2 in both pre- and postsynaptic compartments. **c.** PLA-FERMT2/APP puncta were observed at the synapses stained for post- and presynaptic markers. **d.** Normalized average slope of fEPSP evoked during input-output (I/O) responses in stratum radiatum of area CA1 with Schaffer collateral stimulation from sham control (shNT) and after viral injection of the indicated lentivirus. **e.** Examples of fEPSP traces during baseline (light line) and 30-60 min post LTP induction (dark line). **f.** Time course of the average slope of elicited fEPSP responses following LTP induction by a tetanic stimulation protocol at hippocampal CA1 synapses from 5 mice after viral injection. Time-point 0 represents the delivery of tetanic stimulations. Slopes of each fEPSP are normalized to baseline and plotted against time. **g.** Box plots of the average slope response during 30-60 min post LTP induction. N = 5 mice; 2 slices per animal. Unpaired t-test; * p<0.05, ** p<0.01.

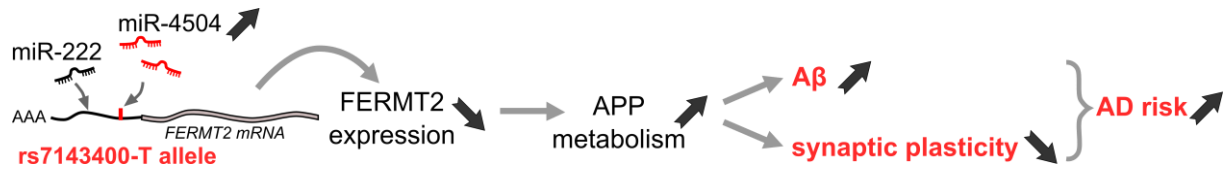


Fig 8. Increase of miR-4504 observed in AD brains could impact *FERMT2* expression for individuals carrying the rs7143400-T allele. The down-regulation of *FERMT2* in neurons might modulate APP metabolism increasing A β production and impairing synaptic plasticity.